

Highly anisotropic resistivities in the double-exchange model for strained manganites

Shuai Dong,^{1,2} Seiji Yunoki,^{3,4} Xiaotian Zhang,^{5,6} Cengiz Şen,^{5,6} J.-M. Liu,^{2,7} and Elbio Dagotto^{5,6}

¹*Department of Physics, Southeast University, Nanjing 211189, China*

²*Nanjing National Laboratory of Microstructures, Nanjing University, Nanjing 210093, China*

³*Computational Condensed Matter Physics Laboratory, RIKEN, Wako, Saitama 351-0198, Japan*

⁴*CREST, Japan Science and Technology Agency (JST), Kawaguchi, Saitama 332-0012, Japan*

⁵*Department of Physics and Astronomy, University of Tennessee, Knoxville, Tennessee 37996, USA*

⁶*Materials Science and Technology Division, Oak Ridge National Laboratory, Oak Ridge, Tennessee 32831, USA*

⁷*International Center for Materials Physics, Chinese Academy of Sciences, Shenyang 110016, China*

(Dated: May 24, 2010)

The highly anisotropic resistivities in strained manganites are theoretically studied using the two-orbital double-exchange model. At the nanoscale, the anisotropic double-exchange and Jahn-Teller distortions are found to be responsible for the robust anisotropic resistivities observed here via Monte Carlo simulations. An unbalanced in the population of orbitals caused by strain is responsible for these effects. In contrast, the anisotropic superexchange is found to be irrelevant to explain our results. Our model study suggests that highly anisotropic resistivities could be present in a wide range of strained manganites, even without (sub)micrometer-scale phase separation. In addition, our calculations also confirm the formation of anisotropic clusters in phase-separated manganites, which magnifies the anisotropic resistivities.

PACS numbers: 75.47.Lx, 71.70.Ej, 75.30.Gw

I. INTRODUCTION

Strongly correlated electronic materials, which are well known for the presence of complex phase competitions involving the spin, charge, and orbital degrees of freedom,¹ are promising candidates to be used in new multifunctional devices.² Typically, in materials such as manganites with the colossal magnetoresistance (CMR), there are several phases with free energies that are quite close to one another but their individual physical properties can be rather different.³ Therefore, colossal responses to external perturbations, including the CMR⁴ and colossal electroresistance (CER),⁵ can and do occur in some manganites. During the past decade, theoretical studies on manganites have addressed many of these colossal responses, such as CMR,^{6–9} CER,^{10,11} surface reconstructions,^{12–15} and disorder effects.^{16–24}

In addition, the effects of strain on the properties of manganites and other complex oxides is attracting increasing attention due to the rapidly expanding research interests in complex oxides heterostructures.^{25,26} In fact, phase transitions driven by strains have been discussed in manganite thin films for several years.^{27–35} The physical mechanism of these phase transition is mostly orbital-order-mediated.^{36–39} For example, according to density functional theory (DFT) calculations, the ground states of $\text{LaMnO}_3/\text{SrMnO}_3$ superlattices can be tuned between A-type antiferromagnetic, ferromagnetic, and C-type antiferromagnetic phases when the ratio c/a is in the range $0.96 \sim 1.04$, where c (a) is the out-of-plane (in-plane) lattice constant.³⁸ Even for LaMnO_3 itself, the ground state may become ferromagnetic (FM) if the $|3x^2 - r^2| > |3y^2 - r^2|$ type orbital order is fully suppressed in the cubic lattice, according to both the DFT and model calculations.^{36,39}

Very recently, Ward *et al.* have observed high anisotropic resistivities in strained $\text{La}_{5/8-x}\text{Pr}_x\text{Ca}_{3/8}\text{MnO}_3$ (LPCMO) thin films.⁴⁰ LPCMO is a prototype phase-separated material.⁴¹ The coexistence of FM and charge-ordered-insulating (COI) clusters at the (sub)micrometer-scale can seriously affect the electric transport properties, especially the metal-insulator transition (MIT). The electric conductance in the phase-separated LPCMO is dominated by the percolation mechanism.^{41,42} For example, giant discrete steps in the MIT and a reemergent MIT occur in an artificially created microstructure of LPCMO when the size confinements in two directions become comparable to the phase-separated cluster sizes.^{43,44} Therefore, Ward *et al.* proposed that the anisotropic percolation might be responsible for the highly anisotropic resistivities in strained LPCMO.⁴⁰ Also, our previous simulation of CER predicted anisotropic resistivities due to the electric-field-driven anisotropic percolation in phase-separated manganites.¹¹

Then, two interesting questions arise: (1) how does strain drive the anisotropic percolation in the LPCMO films? And, more importantly, (2) can the large anisotropies occur in more standard CMR materials with nanometer-scale phase competition or even with bicritical clean-limit phase diagrams? Therefore, to setup a study to be used as a reference for future research it is interesting to investigate theoretically with model Hamiltonians the magnitude of the anisotropy in transport induced by strain in cases where phase competition is present, but also where phase separation is not. In other words, it is important to study regimes where in the clean limit (no quenched disorder) a first-order transition separates the two competing states, typically a metal and an insulator, inducing a CMR effect in a narrow range of

parameters, but where phase separation is not present. This calculation will allow us to disentangle the effects of mere strain on a clean limit model in the regime of phase competition from the effects of strain on a truly phase separated state. More basically, these investigations are important to move beyond the micrometer-scale to find the microscopic origin of anisotropic resistivities in generic strained manganites.

II. MODELS AND TECHNIQUES

In this paper, the two-orbital double-exchange (DE) model will be employed to study the anisotropic resistivities in strained manganites. In the past decade, the DE model has been extensively studied and it proved to be a quite reasonable model to describe perovskite manganites.³ In Ward *et al.*'s experiments, the anisotropic strain field splits the in-plane lattice constants along the [100] and [010] axes in the pseudocubic convention (or the [101] and $\bar{1}01$ axes in the orthorhombic *Pnma* convention). Thus, a modified model has to be developed to reflect the features of this strained lattice, since most previous model studies were done on cubic or square lattices.

As a well-accepted approximation for manganite models, an infinite Hund coupling is here adopted. With this useful simplification, the DE model Hamiltonian reads:

$$\begin{aligned}
 H = & - \sum_{\langle ij \rangle}^{\alpha\beta} t_{\alpha\beta}^{\vec{r}} (\Omega_{ij} c_{i\alpha}^\dagger c_{j\beta} + H.c.) + \sum_{\langle ij \rangle} J_{\text{AF}}^{\vec{r}} \vec{S}_i \cdot \vec{S}_j \\
 & + \lambda \sum_i (-Q_1 n_i + Q_2 \tau_{xi} + Q_3 \tau_{zi}) \\
 & + \frac{1}{2} \sum_i (2Q_1^2 + Q_2^2 + Q_3^2). \quad (1)
 \end{aligned}$$

In the above model Hamiltonian, the first term is the standard DE interaction. α and β denote the two Mn e_g -orbitals a ($|x^2 - y^2\rangle$) and b ($|3z^2 - r^2\rangle$). c_{ia} (c_{ia}^\dagger) annihilates (creates) an e_g electron at orbital α of site i , with its spin parallel to the localized t_{2g} spin \vec{S}_i . The nearest-neighbor (NN) hopping direction is denoted by \vec{r} . The Berry phase Ω_{ij} generated by the infinite Hund coupling equals $\cos(\theta_i/2)\cos(\theta_j/2) + \sin(\theta_i/2)\sin(\theta_j/2)\exp[-i(\phi_i - \phi_j)]$, where θ and ϕ are the polar and azimuthal angles of the t_{2g} spins, respectively. In strained manganites, an elongated lattice constant gives rise to more straight Mn-O-Mn bonds, thus enhancing the FM DE interaction. To mimic this effect, the in-plane DE hopping amplitudes $t_{\alpha\beta}^{\vec{r}}$ have to be set as:

$$\begin{aligned}
 t^x &= \begin{pmatrix} t_{aa}^x & t_{ab}^x \\ t_{ba}^x & t_{bb}^x \end{pmatrix} = \frac{t_0^x}{4} \begin{pmatrix} 3 & -\sqrt{3} \\ -\sqrt{3} & 1 \end{pmatrix} \\
 t^y &= \begin{pmatrix} t_{aa}^y & t_{ab}^y \\ t_{ba}^y & t_{bb}^y \end{pmatrix} = \frac{t_0^y}{4} \begin{pmatrix} 3 & \sqrt{3} \\ \sqrt{3} & 1 \end{pmatrix}. \quad (2)
 \end{aligned}$$

In the rest of the manuscript, t_0^x is taken as the energy unit t_0 and $A_t = t_0^y/t_0^x - 1$ is defined to characterize the degree of anisotropy of the DE interaction.

The second term of the model Hamiltonian is the antiferromagnetic (AFM) superexchange (SE) interaction between NN t_{2g} spins. The SE coefficient J_{AF} could also become anisotropic in the strained lattices, which is here characterized by $A_J = J_{\text{AF}}^x/J_{\text{AF}}^y - 1$.

The third term of the model stands for the electron-lattice coupling. λ is a dimensionless coefficient and n_i is the e_g electronic density at site i . Q s are phonons, including the Jahn-Teller (JT) modes (Q_2 and Q_3) and the breathing mode (Q_1): $Q_1 = (\delta_x + \delta_y + \delta_z)/\sqrt{3}$, $Q_2 = (\delta_x - \delta_y)/\sqrt{2}$, and $Q_3 = (-\delta_x - \delta_y + 2\delta_z)/\sqrt{6}$, where δ stands for the length change of the oxygen coordinates in the Mn-O-Mn bonds along the axes directions. τ is the orbital pseudospin operator, namely $\tau_x = c_a^\dagger c_b + c_b^\dagger c_a$ and $\tau_z = c_a^\dagger c_a - c_b^\dagger c_b$. The last term is the lattice elastic energy. Note that the model used here induces cooperative distortions of the oxygen positions.

The above model Hamiltonian is numerically solved via the Monte Carlo (MC) simulation on a two-dimensional 8×8 lattice. The reason for this restriction to a two-dimensional geometry is simply practical: simulations in three-dimensional lattices are very demanding computationally. Thus, here δ_z is set to zero and our effort will only focus on the in-plane anisotropy. Using standard periodic boundary conditions (PBCs), $\langle Q_1 \rangle$, $\langle Q_2 \rangle$, and $\langle Q_3 \rangle$ (if $\langle \rangle$ stands for averages over the whole lattice) equals to zero. However, to simulate the strain effect in the JT distortion, *anisotropic* PBCs (aPBCs) should be introduced to the lattice. In the aPBCs for 2D lattices, $\langle Q_2 \rangle$ is set as a constant which can be nonzero, while $\langle Q_1 \rangle$ and $\langle Q_3 \rangle$ remain zero. To characterize this anisotropic JT distortion, the quantity A_Q is defined as $-\langle Q_2 \rangle / (2\sqrt{3})$.

In Ward *et al.*'s experiments, the difference between the in-plane lattice constants is small ($\sim 0.2 - 0.3\%$).⁴⁰ Correspondingly, the anisotropies of interactions should be weak, implying that A_t , A_J , and A_Q must be small quantities in our study.

In our MC simulations, the average e_g density $\langle n \rangle$ is chosen as 0.75. As discussed in previous literature, to obtain the MIT and CMR effects, the parameters (J_{AF} , λ) should be chosen to be near the phase boundaries between FM and AFM COI phases.^{8,9} This fine tuning of couplings could be avoided by introducing quenched disorder, but our study will be conducted in the clean limit to setup a benchmark to decide on the origin of strain induced transport anisotropies that are investigated experimentally. According to the phase diagram of the two-orbital DE model for $\langle n \rangle = 0.75$,⁴⁵ the parameters $J_{\text{AF}} = 0.09$ and $\lambda = 1.2$ are suitable and they are here adopted as the default ones in our simulation, unless other parameters are explicitly used. In fact, other sets of parameters near the default ones have also been partially tested and no qualitative differences have been found. Thus, this choice of parameters do not alter the

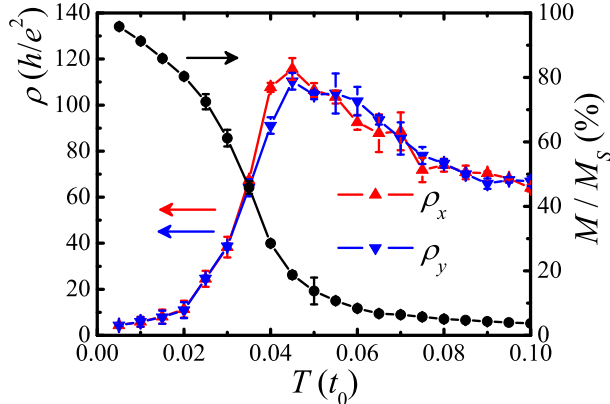


FIG. 1. (Color online) MC simulated resistivities (triangles) and magnetization (dots) for a square 8×8 isotropic lattice ($A_t = 0$, $A_J = 0$, and $A_Q = 0$), as a function of T .

general validation of our results and conclusions, at least qualitatively. In the MC simulation, the first 10^4 MC steps are used to reach thermal equilibrium and another 2×10^4 MC steps are used for measurements.

The dc conductances, which are calculated using the Kubo formula, are in units of e^2/h , where e is the elementary charge and h is the Planck's constant.⁴⁶ The resistivities are the reciprocals of MC averaged conductances. The normalized magnetization (M) is obtained from the spin structure factor $S(\vec{k})$, at $\vec{k} = (0, 0)$.¹⁵

III. RESULTS AND DISCUSSION

To start the discussion of results, the original state without any anisotropic contribution is simulated as a reference. The resistivities along both the x and y directions (ρ_x and ρ_y) are calculated as a function of temperature (T), as shown in Fig. 1. As expected, ρ_x and ρ_y are almost identical in the whole T range. The small differences between ρ_x and ρ_y are from statistical fluctuations during the MC simulation, and these differences should converge to zero with increasing MC simulation times. With this set of parameters, both ρ_x and ρ_y show a MIT with increasing temperature at $T_{\text{MI}} \sim 0.045t_0$, which is the same approximate location as our estimation for the Curie temperature (T_C), according to the $M - T$ curve. For a typical manganite with a MIT under zero magnetic field, t_0 is roughly estimated to be in the range $0.4 - 0.5$ eV.^{15,39} Thus, $T_{\text{MI}} \sim 200 - 260$ K in agreement with bulk measurements. Therefore, the set of parameters ($J_{\text{AF}} = 0.09$, $\lambda = 1.2$) used here is suitable to describe typical manganites, such as $\text{La}_{1-x}\text{Ca}_x\text{MnO}_3$.

In the following, we will apply the aforementioned three anisotropic interactions one by one into the model simulation to clarify their respective roles. First, let us

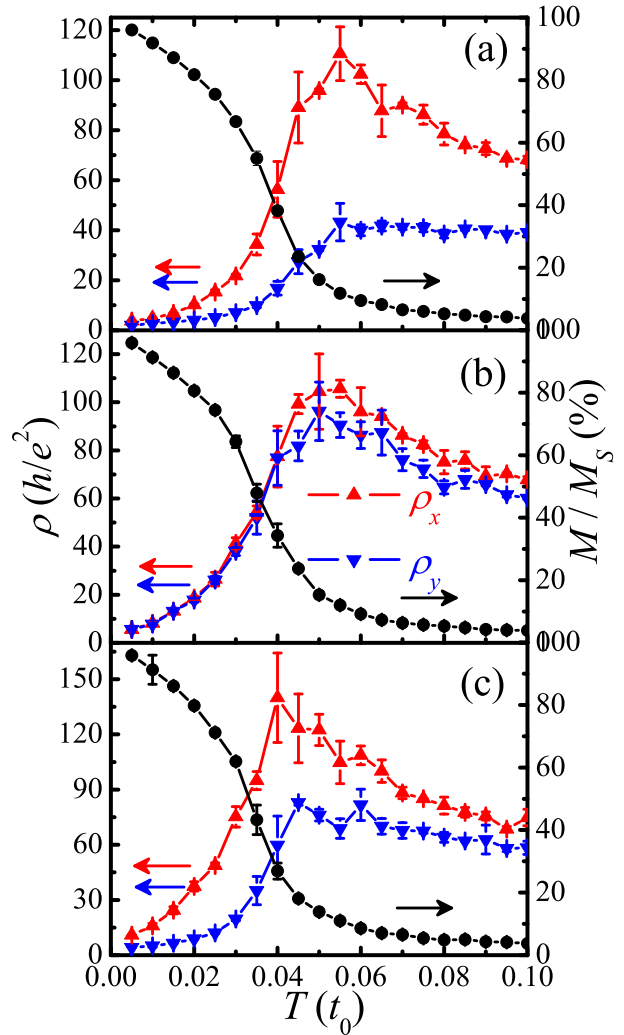


FIG. 2. (Color online) MC simulated resistivities (triangles) and magnetization (dots) for strained lattices, as a function of T . (a) Only the anisotropic DE interaction is here considered ($A_t = 0.1$, $A_J = 0$, and $A_Q = 0$). (b) Only the anisotropic SE interaction is considered ($A_t = 0$, $A_J = 0.1$, and $A_Q = 0$). To maintain the presence of a metal-insulator transition J_{AF}^y must be slightly reduced to 0.086. (c) Only the strained JT distortion is considered ($A_t = 0$, $A_J = 0$, and $A_Q = 0.01$).

consider the anisotropic DE interaction. For this purpose, A_t is set to 0.1 while other parameters are kept the same as the original ones. In other words, the DE hopping amplitude along the y direction is made 10% larger than that along the x direction, because of the presence of more straight Mn-O-Mn bonds along the y axis. The resistivities and magnetization of this strained lattice are shown in Fig. 2(a) as a function of T . ρ_x shows a MIT similar to the original one while ρ_y is now considerably suppressed in magnitude. Thus, a high degree of anisotropic resistivities can be obtained using an

anisotropy A_t in the hoppings which is only 0.1. Interestingly, although the difference between ρ_x and ρ_y are substantial, the differences in the T_{MI} 's shown in ρ_x and ρ_y are not obvious in this $A_t = 0.1$ case. Comparing with the original one, T_C and T_{MI} actually simultaneously raise to $\sim 0.055t_0$ due to the increase in t_0^y .

Next, the anisotropic SE is taken into account. A_t is restored to 0, while A_J is set to 0.1. In this case, J_{AF}^y has to be weakened slightly to preserve the presence of an MIT, otherwise the system becomes insulating in the whole T range if J_{AF}^y remains at 0.09. Thus, for this case the new values $J_{\text{AF}}^y = 0.085$ and $J_{\text{AF}}^x = 0.0935$ are adopted. The MC simulated resistivities and magnetization for this strained lattice are shown in Fig. 2(b), as a function of T . The T_{MI} remains isotropic and coincides with $T_C \sim 0.05t_0$. In contrast to the DE case, the differences between ρ_x and ρ_y are much smaller, especially below T_C (or T_{MI}): ρ_y is only slightly lower than ρ_x above $0.04t_0$, and they are almost identical below $0.04t_0$. Then we conclude that the effect of an anisotropic SE is much weaker than the case of an anisotropic DE, when their anisotropic ratios are the same.

Finally, it is necessary to address the effect of anisotropies in the JT sector, for completeness. In a distorted oxygen octahedron, the two e_g orbitals are not degenerate anymore. For instance, when the lattice constants along the x and y axes are different, as in the Ward *et al*'s strained manganites thin films, $\langle Q_2 \rangle$ is no longer zero. This nonzero $\langle Q_2 \rangle$ mode induces an orbital-state "preference" over the whole lattice. With $A_t = 0$, $A_J = 0$, and $A_Q = 0.01$, the MC simulated resistivities and magnetization are shown in Fig. 2(c), as a function of T . Similar to the case of an anisotropic DE, there is now a substantial difference between ρ_x and ρ_y . In addition, the T_{MIS} of the ρ_x and ρ_y curves becomes anisotropic: the lower resistivity curve has a higher T_{MI} , in agreement with the experiments.⁴⁰

To further clarify the anisotropic resistivities observed here, the relative percentage difference (δ) between ρ_x and ρ_y (defined as $\delta = (\rho_x - \rho_y)/\rho_y \times 100\%$) is calculated for each of the three cases discussed above, as shown in Fig. 3(a). For the original isotropic and the $A_J = 0.1$ cases, the values of δ are very small ($< \pm 20\%$) in the whole temperature range, as expected from Figs. 1 and 2(b). In contrast, for the $A_t = 0.1$ and $A_Q = 0.01$ cases, the situation is different. With increasing T from low temperatures, δ s first increases. After each case reaches a robust peak of 200 – 300%, then they decrease with further increases in T . Interestingly, for both these two cases, the corresponding T s of the peaks found in δ are slightly lower than the corresponding T_C s and T_{MIS} s, in agreement with the experimental results.⁴⁰

To understand the physical mechanism leading to the anisotropic resistivities the orbital properties of the strained states, characterized by the average values of the pseudo-spin orbital operator $\langle \tau_x \rangle$, are also calculated, as shown in Fig. 3(b). The occupation difference between the $|3y^2 - r^2\rangle$ and $|3x^2 - r^2\rangle$ components is in pro-

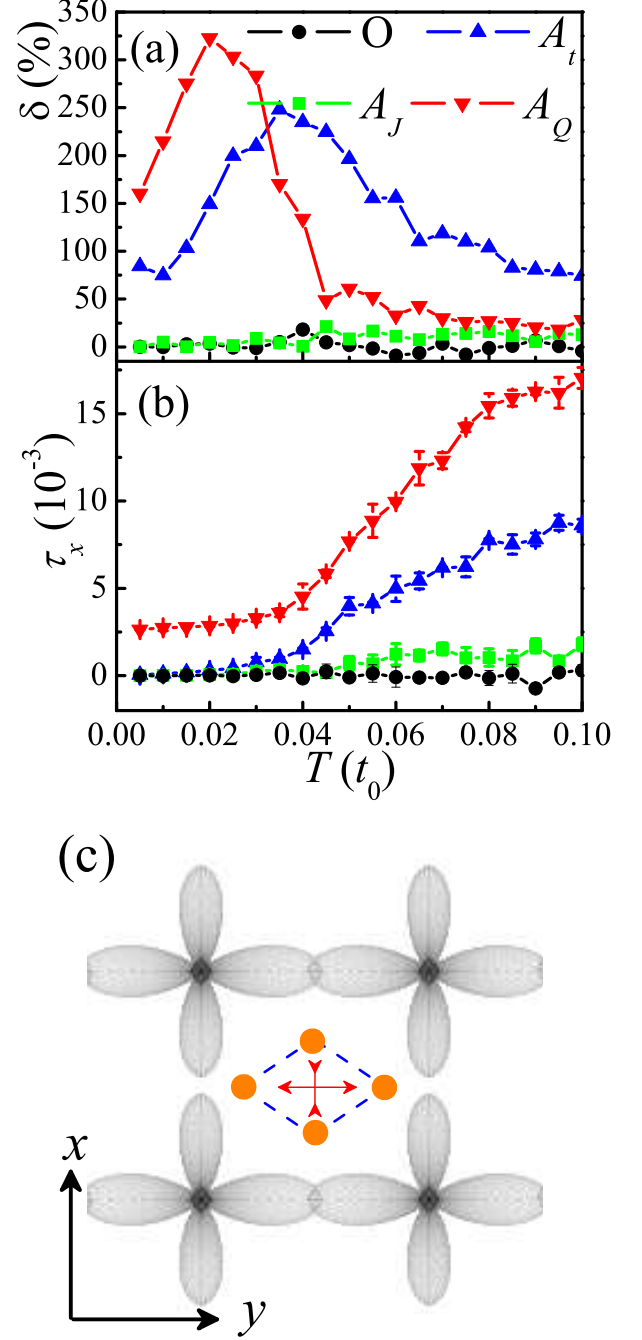


FIG. 3. (Color online) (a) Relative percentage differences between ρ_x and ρ_y , as a function of T , for the cases indicated. O stands for original isotropic. (b) The average values of $\langle \tau_x \rangle$, as a function of T . (c) Sketch of the effect of strain on the orbitals. To better distinguish the orbital-leaves along the x and y directions, here $\langle \tau_x \rangle / \langle \tau_y \rangle$ is magnified to 0.1. In the sketch, the overlap of electronic clouds becomes stronger along the y direction and weaker along the x direction. Thus, the conductances, which are in proportion to the overlaps, become anisotropic. Note that the real overlaps are indirect and mediated by oxygens (not shown here). Inset: sketch of an oxygen octahedron's in-plane distortion.

portion to $\langle \tau_x \rangle$. The values of $\langle \tau_x \rangle$ for the original isotropic case fluctuate around zero in the whole T range analyzed, implying that the weights of the $|3y^2 - r^2\rangle$ and $|3x^2 - r^2\rangle$ orbitals are equal, as expected by symmetry. For the $A_J = 0.1$ cases, $\langle \tau_x \rangle$ still remains very small, implying that the anisotropic J_{AF} used is not relevant to affect substantially the orbital composition of the state. In fact, both these two cases give rise to (almost) isotropic resistivities. In clear contrast, for the $A_t = 0.1$ and $A_Q = 0.01$ cases, finite values for $\langle \tau_x \rangle$ are observed at high T , which are gradually suppressed by the FM transitions with decreasing T . For the $A_Q = 0.01$ case, the finite $\langle \tau_x \rangle$ is mainly caused by the JT distortion, which remains finite at low T as long as the lattice is anisotropically distorted. However, the finite $\langle \tau_x \rangle$ for the $A_t = 0.1$ case is caused by the enhanced DE process along the y direction. Namely, it is a DE mediated polarization of the orbital occupancy. Thus, for the fully FM state at low T , this DE mediated orbital rearrangement is largely suppressed to near zero, which is different from the results obtained for the JT distortion case. In summary, in our simulation the large anisotropy of the resistivity emerges in those cases where there is an unbalanced in the orbital state population, as sketched in Fig. 3(c), although the value of δ is not linearly dependent on $\langle \tau_x \rangle$ in the whole T range. In simple terms, the orbitals that increase their overlaps due to strain are now more populated than the other ones.

Note that all the above simulations were carried out on relatively small 8×8 clusters using clean-limit models and still the anisotropy observed is comparable to that found experimentally. This implies that clean-limit strained manganites can be as anisotropic as phase separated compounds. Therefore, the LPCMO phase separation and classical percolation at the (sub)micrometer scale does not appear to be essential to obtain highly anisotropic resistivities, but of course in the clean limit the strain induced by substrates must be sufficiently large to generate a $A_t = 0.1$ as used here, while for phase-separated compounds this anisotropy arises from phase competition. Thus, the high anisotropic resistivities should be a general properties of manganites and even other complex oxides, as long as the bond lengths/angles are tuned to be sufficiently anisotropic by strain. Further experimental studies on strained oxide films are needed to verify our results.

However, it is important to clarify that in the particular case of large scale phase-separated manganites, the classic percolation mechanism can certainly also contribute to the anisotropic resistivities if the shapes of the FM metallic clusters become anisotropic, as suggested in Ref. 40. In fact, our model can also qualitatively explain the formation of anisotropic FM clusters. To study an individual phase-separated FM cluster embedded in the AFM COI matrix, the ground state energies of FM lattices with *open* boundary conditions can be calculated directly. For simplicity, all Q_{2i} are set to be uniform (and equal to $\langle Q_2 \rangle$) and all spins are aligned to be

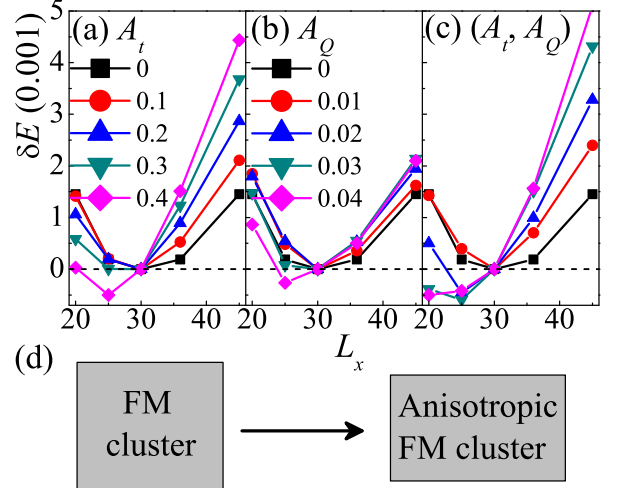


FIG. 4. (Color online) Energy differences of the ground states of $L_x \times L_y = 900$ lattices, as a function of L_x . The energy of the $L_x = 30$ lattice is set as the reference point. (a) Results obtained with the anisotropic DE interactions. (b) Results obtained with the strained JT distortions. (c) Results obtained with both the anisotropic DE interactions and strained JT distortions simultaneously active. The values of (A_t, A_Q) in (c) are simultaneously stepped the same as in (a) and (b), respectively. (d) Sketch of the formation of an anisotropic FM cluster, according to (a-c).

perfectly FM. Then, the shape of the FM clusters can be determined by varying the lattice's shape but keeping a constant lattice area. For instance, the energies of lattices with the same area size ($L_x \times L_y = 900$, L_x and L_y are side lengths along the x and y axes, respectively) are shown in Fig. 4(a-c), as a function of L_x . The energy of the 25×36 lattice, which is elongated along the y direction, can be obviously more stable than that of a 30×30 one when $A_t > 0.3$, or $A_Q \geq 0.04$, or $A_t \geq 0.2$ and $A_Q \geq 0.02$ simultaneously. This process is qualitatively sketched in Fig. 4(d). FM clusters with other sizes (e.g. $L_x \times L_y = 576$ and $L_x \times L_y = 1764$) have also been tested, reaching the same conclusion. Thus, it is reasonable to expect similar effects when FM clusters expand to the (sub)micrometer scale, although our microscopic model can not be directly used on such large lattices with the currently available computational capabilities.

Finally, it is important to estimate how large should be the lattice mismatch required for the highly anisotropic resistivities observed here to appear in strained manganites with nanoscale phase separation or in the case of a bicritical phase diagram. According to the well-known Harrison's formula,⁴⁷ the DE hopping t and SE exchange J_{AF} can be estimated to be in proportional to r^{-7} and r^{-14} (r is the Mn-O-Mn's bond length), respectively. Thus t/J_{AF} is in proportion to r^7 . To obtain the values $A_t = 0.1$ and $A_J = 0.1$ used in our simulations, the required lattice mismatch is about 1.4%. Similarly, by

comparing experimental data ($r_l - r_s \sim 0.6 \text{ \AA}$, where r_l and r_s are long and short bonds, respectively)⁴⁸ and theoretical parameters ($|\lambda/Q_2| = 1.5$)⁴⁹ for the JT distortions in $R\text{MnO}_3$, the parameter $A_Q = 0.01$ used here is estimated as $\sim 0.45\%$. It should be noted that the required strain (lattice mismatch in real films, or (A_t, A_Q) in our simulations) depends on the particular materials under study (or, equivalently, the actual values of the parameters (J_{AF}, λ) in our simulations). The anisotropies are more sensitive to strain when the system moves closer to the phase boundary between the FM and COI phases. With this idea in mind, it is natural that the anisotropies of LPCMO films can be notorious even if the lattice mismatch is small in average ($0.2 - 0.3\%$ in Ward *et al.*'s experiments), because LPCMO is precisely at the FM-COI phase boundary. According to our simulations, the highly anisotropic resistivities are also expected in other strained CMR manganites films (even without phase separation), although the required strain might be somewhat larger than for the LPCMO case.

IV. CONCLUSIONS

In conclusion, the high anisotropic resistivities of strained manganites films were studied using microscopic models. For this purpose, the two-orbital double-exchange model was modified to include the strain contributions. In this revised model, the anisotropic Jahn-Teller distortion was emphasized, in addition to the anisotropic exchanges. The results of our MC sim-

ulation shows that the highly anisotropic resistivities are associated with an unbalanced in orbital populations which is driven by the anisotropic double-exchange and anisotropic Jahn-Teller distortions. In contrast, the anisotropic superexchange was not found to be a dominant driving force for the anisotropic resistivities. The observed high anisotropic resistivities in our simulation did not rely on phase separation at the (sub)microscopic scale. Therefore, it is expected that this anisotropic state could be realized in a variety of manganites and other complex oxides as well, if a sufficiently large lattice mismatch can be achieved in the growth of the manganite films. In addition, for the particular case of phase-separated manganites, our model investigations suggest that the anisotropic double-exchange and strained Jahn-Teller distortions could indeed reshape the ferromagnetic clusters, thus inducing an anisotropic percolation and concomitant anisotropic resistivity that further enhances these effects.

ACKNOWLEDGMENTS

We thank T.Z. Ward and J. Shen for fruitful discussions. Work was supported by the 973 Projects of China (2006CB921802, 2009CB623303) and the National Science Foundation of China (50832002). S.Y. was supported by CREST-JST. X.T.Z., C.S., and E.D. were supported by the USA National Science Foundation grant DMR-0706020 and by the Division of Materials Science and Engineering, Office of Basic Energy Sciences, U.S. Department of Energy.

-
- ¹ E. Dagotto, Science **309**, 257 (2005).
 - ² H. Takagi and H. Y. Hwang, Science **327**, 1601 (2010).
 - ³ E. Dagotto, T. Hotta, and A. Moreo, Phys. Rep. **344**, 1 (2001).
 - ⁴ Y. Tokura, Rep. Prog. Phys. **69**, 797 (2006).
 - ⁵ A. Asamitsu, Y. Tomioka, H. Kuwahara, and Y. Tokura, Nature (London) **388**, 50 (1997).
 - ⁶ J. Burgu, A. Moreo, and E. Dagotto, Phys. Rev. Lett. **92**, 097202 (2004).
 - ⁷ C. Şen, G. Alvarez, H. Aliaga, and E. Dagotto, Phys. Rev. B **73**, 224441 (2006).
 - ⁸ C. Şen, G. Alvarez, and E. Dagotto, Phys. Rev. Lett. **98**, 127202 (2007).
 - ⁹ R. Yu, S. Dong, C. Şen, G. Alvarez, and E. Dagotto, Phys. Rev. B **77**, 214434 (2008).
 - ¹⁰ S. Dong, C. Zhu, Y. Wang, F. Yuan, K. F. Wang, and J.-M. Liu, J. Phys.: Condens. Matter **19**, 266202 (2007).
 - ¹¹ S. Dong, H. Zhu, and J.-M. Liu, Phys. Rev. B **76**, 132409 (2007).
 - ¹² M. J. Calderón, L. Brey, and F. Guinea, Phys. Rev. B **60**, 6698 (1999).
 - ¹³ Z. Fang and K. Terakura, J. Phys. Soc. Jpn. **70**, 3356 (2001).
 - ¹⁴ S. Dong, F. Gao, Z. Q. Wang, J.-M. Liu, and Z. F. Ren, Appl. Phys. Lett. **90**, 082508 (2007).
 - ¹⁵ S. Dong, R. Yu, S. Yunoki, J.-M. Liu, and E. Dagotto, Phys. Rev. B **78**, 064414 (2008).
 - ¹⁶ Y. Motome, N. Furukawa, and N. Nagaosa, Phys. Rev. Lett. **91**, 167204 (2003).
 - ¹⁷ C. Şen, G. Alvarez, and E. Dagotto, Phys. Rev. B **70**, 064428 (2004).
 - ¹⁸ H. Aliaga, D. Magnoux, A. Moreo, D. Poilblanc, S. Yunoki, and E. Dagotto, Phys. Rev. B **68**, 104405 (2003).
 - ¹⁹ S. Kumar and P. Majumdar, Phys. Rev. Lett. **91**, 246602 (2003).
 - ²⁰ S. Kumar and P. Majumdar, Phys. Rev. Lett. **94**, 136601 (2005).
 - ²¹ K. Pradhan, A. Mukherjee, and P. Majumdar, Phys. Rev. Lett. **99**, 147206 (2007).
 - ²² S. Kumar and A. P. Kampf, Phys. Rev. Lett. **100**, 076406 (2008).
 - ²³ J. Salafranca, M. J. Calderón, and L. Brey, Phys. Rev. B **77**, 014441 (2008).
 - ²⁴ X. Chen, S. Dong, K. F. Wang, J.-M. Liu, and E. Dagotto, Phys. Rev. B **79**, 024410 (2009).
 - ²⁵ E. Dagotto, Science **318**, 1076 (2007).
 - ²⁶ J. Mannhart and D. G. Schlom, Science **327**, 1607 (2010).
 - ²⁷ Y. Konishi, Z. Fang, M. Izumi, T. Manako, M. Kasai, H. Kuwahara, M. Kawasaki, K. Terakura, and Y. Tokura, J. Phys. Soc. Jpn. **68**, 3790 (1999).

- ²⁸ J. Dho, Y. N. Kim, Y. S. Hwang, J. C. Kim, and N. H. Hur, Appl. Phys. Lett. **82**, 1434 (2003).
- ²⁹ J. Klein, J. B. Philipp, D. Reisinger, M. Opel, A. Marx, A. Erb, L. Alff, and R. Gross, J. Appl. Phys. **93**, 7373 (2003).
- ³⁰ K. H. Ahn, T. Lookman, and A. R. Bishop, Nature (London) **428**, 401 (2004).
- ³¹ W. Wu, C. Israel, N. Hur, S. Park, S.-W. Cheong, and A. D. Lozanne, Nature Mater. **5**, 881 (2006).
- ³² H. Yamada, M. Kawasaki, T. Lottermoser, T. Arima, and Y. Tokura, Appl. Phys. Lett. **89**, 052506 (2006).
- ³³ T. Dhakal, J. Tosado, and A. Biswas, Phys. Rev. B **75**, 092404 (2007).
- ³⁴ M. C. Dekker, A. D. Rata, K. Boldyreva, S. Oswald, L. Schultz, and K. Dörr, Phys. Rev. B **80**, 144402 (2009).
- ³⁵ Y. Ding, D. Haskel, Y.-C. Tseng, E. Kaneshita, M. van Veenendaal, J. F. Mitchell, S. V. Sinogeikin, V. Prakapenka, and H.-K. Mao, Phys. Rev. Lett. **102**, 237201 (2009).
- ³⁶ H. Sawada, Y. Morikawa, K. Terakura, and N. Hamada, Phys. Rev. B **56**, 12154 (1997).
- ³⁷ Z. Fang, I. V. Solovyev, and K. Terakura, Phys. Rev. Lett. **84**, 3169 (2000).
- ³⁸ B. R. K. Nanda and S. Satpathy, Phys. Rev. B **78**, 054427 (2008).
- ³⁹ S. Dong, R. Yu, S. Yunoki, G. Alvarez, J.-M. Liu, and E. Dagotto, Phys. Rev. B **78**, 201102(R) (2008).
- ⁴⁰ T. Z. Ward, J. D. Budai, Z. Gai, J. Z. Tischler, L. F. Yin, and J. Shen, Nature Phys. **5**, 885 (2009).
- ⁴¹ M. Uehara, S. Mori, C. H. Chen, and S.-W. Cheong, Nature (London) **399**, 560 (1999).
- ⁴² M. Mayr, A. Moreo, J. A. Vergés, J. Arispe, A. Feiguin, and E. Dagotto, Phys. Rev. Lett. **86**, 135 (2001).
- ⁴³ H.-Y. Zhai, J. X. Ma, D. T. Gillaspie, X. G. Zhang, T. Z. Ward, E. W. Plummer, and J. Shen, Phys. Rev. Lett. **97**, 167201 (2006).
- ⁴⁴ T. Z. Ward, S. Liang, K. Fuchigami, L. F. Yin, E. Dagotto, E. W. Plummer, and J. Shen, Phys. Rev. Lett. **100**, 247204 (2008).
- ⁴⁵ S. Dong, R. Yu, J.-M. Liu, and E. Dagotto, Phys. Rev. Lett. **103**, 107204 (2009).
- ⁴⁶ J. A. Vergés, Comput. Phys. Commun. **118**, 71 (1999).
- ⁴⁷ W. A. Harrison, *Electronic Structure and the Properties of Solids* (New York: Dover, 1989).
- ⁴⁸ J. A. Alonso, M. J. Martínez-Lope, M. T. Casais, and M. T. Fernández-Díaz, Inorg. Chem. **39**, 917 (2000).
- ⁴⁹ S. Dong, R. Yu, S. Yunoki, J.-M. Liu, and E. Dagotto, Phys. Rev. B **78**, 155121 (2008).